

Article

An Investigation into the Microstructures and Mechanical Properties of a TIG Welding Joint in Ti-4Al-2V Titanium Alloy

Yao Chen ¹, Xiao Liu ¹, Zhendi Zhang ¹, Kaiqing Wang ¹, Shanglin Zhang ¹, Bingnan Qian ^{1,2,3}, Jun Wu ^{1,*} and Li Wang ¹

¹ National Key Laboratory of Nuclear Reactor Technology, Nuclear Power Institute of China, Chengdu 610041, China; cz125115@163.com (Y.C.)

² Shenzhen Key Laboratory of Intelligent Robotics and Flexible Manufacturing Systems, Southern University of Science and Technology, Shenzhen 518055, China

³ Department of Mechanical and Energy Engineering, Southern University of Science and Technology, Shenzhen 518055, China

* Correspondence: wujunscu@163.com

Abstract: The Ti-4Al-2V (wt. %) titanium alloy has garnered widespread applications across diverse fields due to its exceptional strength-to-weight ratio, high toughness, specific strength, and corrosion resistance. The welding of Ti-4Al-2V titanium alloy components is often necessary in manufacturing processes, where the reliability of a welded joint critically influences the overall service life of these components. Consequently, a comprehensive understanding of the welded joint's microstructure and mechanical properties is imperative. In this study, Ti-4Al-2V titanium alloy was welded using multi-layer and multi-pass TIG welding techniques, and a detailed examination was conducted to analyze the microstructure and grain morphology of each microzone of the welded joint. The results revealed the presence of an initial α phase and a secondary lamellar α phase in the heat affected zone (HAZ). Meanwhile, the fusion zone (FZ) primarily comprised a coarse secondary α phase and a small amount of an acicular martensitic α' phase. Both the recrystallization zone and the superheated zone exhibited a distinct preferred orientation, with grains smaller than 10 μm accounting for 65.9% and 55.1%, respectively. To assess the mechanical properties of the various microzones and the typical microstructure within the welded joint, nanoindentation tests were performed. The results indicated that the recrystallization zone possessed a higher nanohardness (3.753 GPa) than the incomplete recrystallization zone (3.563 GPa) and the superheated zone (3.48 GPa). Among all the microzones, the FZ exhibited the lowest average nanohardness (3.058 GPa). Notably, the basket-weave microstructure demonstrated the highest average nanohardness, reaching 3.93 GPa. This was followed by the fine-grain microstructure, which possessed a slightly lower nanohardness. The Widmanstätten microstructure, on the other hand, exhibited the lowest nanohardness among the three microstructures within the HAZ. Therefore, the basket-weave microstructure stands out as the most desirable microstructure to achieve in the welded joint. In summary, this study provides a comprehensive characterization and analysis of the microstructure and properties of Ti-4Al-2V titanium alloy TIG welds, aiming to contribute to the optimization of the TIG welding process for Ti-4Al-2V titanium alloy.

Keywords: Ti-4Al-2V titanium alloy; TIG welding; microstructure; nanoindentation; mechanical properties of microzones



Citation: Chen, Y.; Liu, X.; Zhang, Z.; Wang, K.; Zhang, S.; Qian, B.; Wu, J.; Wang, L. An Investigation into the Microstructures and Mechanical Properties of a TIG Welding Joint in Ti-4Al-2V Titanium Alloy. *Metals* **2024**, *14*, 596. <https://doi.org/10.3390/met14050596>

Academic Editor: Pasquale Russo Spena

Received: 14 April 2024

Revised: 12 May 2024

Accepted: 17 May 2024

Published: 19 May 2024



Copyright: © 2024 by the authors. Licensee MDPI, Basel, Switzerland. This article is an open access article distributed under the terms and conditions of the Creative Commons Attribution (CC BY) license (<https://creativecommons.org/licenses/by/4.0/>).

1. Introduction

The Ti-4Al-2V titanium alloy, a representative near- α phase titanium alloy, has been extensively employed in the manufacturing of ship hulls, nuclear heat exchangers, condensers, and various other components [1,2]. Its widespread application is primarily attributed to its attractive properties, which encompass its strength-to-weight ratio, exceptional specific strength and toughness, outstanding welding characteristics, and robust

corrosion resistance [3,4]. However, the utilization of Ti-4Al-2V titanium alloy components necessitates high-strength joining mechanisms that guarantee sufficient metallurgical and mechanical properties.

Tungsten Inert Gas (TIG) is one of the most commonly utilized welding techniques for titanium alloys, because it produces high-quality welds with a composition closely resembling the parent metal [4–8]. These welds exhibit significant strength and enduring corrosion resistance. However, during the welding process, each microzone of the welded joint experiences uneven heating due to its varying distance from the welding heat source. This inhomogeneous heating leads to alterations in the microstructure and grain morphology, subsequently impacting the mechanical properties of the welded joint and significantly affecting the long-term service performance of the components [9–12]. Especially when Ti-4Al-2V titanium alloy is applied to components of nuclear heat exchanger piping systems, the unevenness in the microstructure of the welded areas can lead to inconsistent corrosion resistance with prolonged use, potentially causing damage to the piping system and affecting the safety and economy of the reactor operations [8,13]. However, there is no systematic study on the microstructure and mechanical properties of Ti-4Al-2V titanium alloy welded joint microzones, especially the different microzones of the HAZ. Therefore, it is imperative to conduct a thorough investigation into the microstructure and to evaluate the mechanical properties, including the hardness and elastic modulus, of Ti-4Al-2V titanium alloy TIG welding joints to ensure their structural integrity and durability during service.

In recent decades, the microstructure and mechanical properties of titanium alloy TIG welded joints have garnered extensive attention. Sundaresan et al. [14] indicated that the original β grains in the heat affected zone (HAZ) of the Ti-6Al-4V titanium alloy undergo notable growth as a result of the thermal cycle associated with TIG welding. Additionally, the microstructure of the fusion zone (FZ) was composed of coarse β grains and acicular α and α' phases. Akhonin et al. [15] investigated the influence of TIG welding on the microstructure and mechanical properties of a VT19 titanium alloy welded joint. Hu et al. [16] demonstrated that the HAZ and FZ of the TC17 titanium alloy TIG welded joint are composed primarily of α' martensite, acicular α , and Widmanstätten $\alpha + \beta$, respectively. The hardness of the FZ is lower than that of the base metal (BM). Babu et al. [17] explored the influence of the welding current on the microstructure and mechanical properties of a Ti-6Al-4V titanium alloy TIG welded joint. Mehdi et al. [18] reported on the microstructure and mechanical properties of a Ti-6Al-4V titanium alloy TIG welded joint, and indicated that the hardness of the FZ decreases with an increase in the residual β phase. Currently, research on titanium alloy TIG welding has predominantly focused on $\alpha + \beta$ titanium alloys, with significantly fewer studies devoted to near- α titanium alloys, especially the Ti-4Al-2V titanium alloy. Furthermore, the majority of studies on welded joints have concentrated their analysis on the overall HAZ, overlooking a comprehensive and systematic examination of the distinct microregions within the HAZ. Consequently, there is a pressing need for additional research to bridge these gaps and foster a deeper comprehension of the microstructure, mechanical properties, and overall performance of titanium alloy TIG welded joints, particularly across diverse alloy types and microregions.

Due to the exceedingly minute dimensions of the various microzones within a welded joint, traditional micronano mechanical testing methods face difficulties in acquiring accurate mechanical properties, especially for an ultrafine microstructure. Nanoindentation, a cutting-edge, non-destructive, reliable, and efficient testing technique, has gained widespread application in the mechanical characterization of materials at the micronano scale [19]. In contrast to traditional mechanical testing methods, nanoindentation enables the precise measurement of the mechanical properties, such as the hardness and elastic modulus, of various regions in the weld specimens at the microscale [20–22]. Chu et al. [21] harnessed nanoindentation technology to delve into the welded joint of titanium–steel clad plates, thereby revealing the mechanical property distribution of intermetallic compounds at the bonding interface. Lan et al. [23] employed nanoindentation to investigate the hardness and elastic modulus of distinct microstructures in a high-strength steel welded joint,

successfully establishing a correlation between the microstructures and the properties of nanoindentation. Chen et al. [24] and Muhammad et al. [25] investigated the nanohardness and elastic modulus of different phases in a titanium alloy welded joint. However, current research on the mechanical properties of typical titanium alloy microstructures remains scarce, with a preponderance of studies focusing solely on the phase nanohardness. Therefore, this study employs nanoindentation technology to establish a dependency between the typical microstructures and mechanical properties of titanium alloy welds.

To ensure the reliability of Ti-4Al-2V titanium alloy TIG welded joints and establish a robust foundation for their future engineering applications, this study has conducted a comprehensive systematic characterization, as well as an in-depth analysis, of the microstructure and properties of a Ti-4Al-2V titanium alloy TIG welded joint. In this study, the microstructural characteristics of the BM, HAZ, and FZ were thoroughly analyzed, with a particular focus on the microstructural features within the various microzones of the HAZ. Utilizing nanoindentation techniques, the overall hardness and elastic modulus of the welded joint were accurately measured. Notably, this study marks the first instance where the nanoindentation hardness and elastic modulus of typical titanium alloy microstructures have been analyzed, thereby establishing a relationship between the microstructure and micromechanical properties of a Ti-4Al-2V titanium alloy TIG welded joint. The results of this study will contribute to the optimization of the TIG welding processes for the Ti-4Al-2V titanium alloy.

2. Material and Methods

2.1. Material and Welding Conditions

The Ti-4Al-2V titanium alloy in the form of an annealed sheet is used as the BM in this study and the same alloy is used as the filler metal. After conducting a thorough analysis of the chemical composition of the Ti-4Al-2V titanium alloy, its main chemical elements are presented in Table 1. In this study, a tungsten electrode with a diameter of 3.5mm was used as the electrode for the TIG welding. Table 2 outlines the welding parameters that were employed to achieve multi-layer and multi-pass automatic TIG welding of the Ti-4Al-2V titanium alloy. The welding experiment was conducted in a shielded atmosphere of 99.99% pure argon, with the argon flow rate controlled at 10–25 L/min. A schematic representation of the Ti-4Al-2V titanium alloy welding joint is shown in Figure 1. As shown in Figure 1, the welding parts are joined together using a lap joint welding method.

Table 1. Measured composition of Ti-4Al-2V titanium alloy (mass fraction, %).

Ti	Al	V	C	O	Fe	Si
base metal	4.2	1.8	0.01	0.09	<0.05	<0.01

Table 2. TIG welding process parameters.

Current (A)	Voltage (V)	Welding Speed (mm/min)	Pulse Time (ms)
60–150	8–10	150	200–200

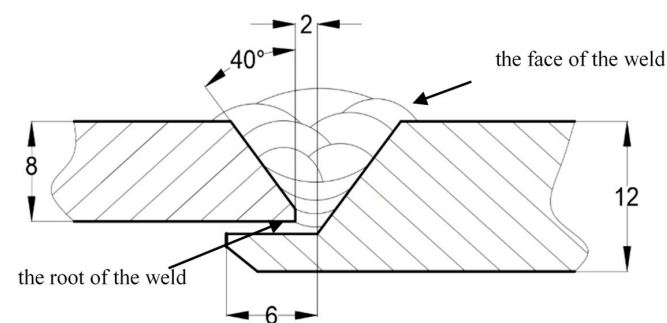


Figure 1. A schematic presentation of the Ti-4Al-2V titanium alloy welding joint (unit: mm).

2.2. Microscopy

Samples encompassing the BM, HAZ, and FZ were wire-cut from TIG weldments using electrical discharge machining for microstructure and microhardness analyses. The sampling rule was as follows: The longitudinal section of the weld should be sampled along the center of the weld, and the sample should include the BM, HAZ, and FZ. The metallographic samples were mechanically ground with wet abrasive paper of varying grit sizes (280, 320, 800, and 1000 grit) and polished using 1 μm Struers diamond suspension paste, followed by a shock polish to eliminate the hardened layer of the surface. Optical microscope (OM) and microhardness test samples were etched using a solution composed of $\text{HF}:\text{HNO}_3:\text{H}_2\text{O}$ in a volume ratio of 1:4:15. The microstructure and grain morphology of the weld joint were characterized by a Leica DMI optical microscope and a JSM-IT500 scanning electron microscope (SEM), equipped with electron backscattered diffraction (EBSD) capabilities.

2.3. Nanoindentation and Vickers Hardness

The nanoindentation tests were conducted utilizing a G200 Nano indentation instrument. These tests were executed with a maximum loading force of 200 mN in the continuous stiffness measurement mode, during which the hardness and modulus data were determined as a function of depth. A Berkovich diamond tip was employed and calibrated prior to testing using a fused quartz reference sample. The indentation procedure involved holding the maximum load for up to 15 s, maintaining the peak load for 10 s, and then unloading at a relatively constant rate. To establish a hardness profile for each weld zone, namely, the BM, HAZ, and FZ, a gradual transition was adopted for the measurements within each microzone. For the BM and HAZ, the nanoindentation measurements were systematically arranged using a 5×5 grid configuration, with a spacing of 1 mm between each indentation point. For the FZ, a finer 10×10 grid configuration was used, maintaining a spacing of 0.5 mm between each indentation point. Furthermore, a 3×3 grid was superimposed on each representative microstructure, with a spacing of 50 nm between each indentation point within the grid. The average value of each microstructure was determined on the basis of the nine measured datapoints.

The Vickers hardness of various microzones within the welded joint of the Ti-4Al-2V titanium alloy was precisely determined using the FALCON500 automated microhardness testing apparatus. The test parameters were standardized, with a loading load set at 50 g and a dwell time of 10 s. The distance between the consecutive measurement points was maintained at 1 mm; for each microzone, five distinct points were evaluated, and their hardness values were averaged to obtain a representative hardness value for that particular microzone.

3. Results and Discussion

The cross-sectional macrograph of the Ti-4Al-2V titanium alloy weld joint is shown in Figure 2. The diagram clearly depicts three distinct regions, namely, the BM, HAZ, and FZ, each of which has been demarcated by dotted lines. Furthermore, the HAZ can be further categorized into three subzones: the incomplete recrystallization zone (marked as area I in Figure 2), the recrystallization zone (marked as area II), and the superheated zone (marked as area III). The subdivision of the HAZ is based on the varying distances of each microzone from the welding heat source. Due to these differing distances and their corresponding influences, significant variations in grain size emerge, enabling a clear distinction between the microzones according to their grain size. The labeled positions I, II, and III represent the centers of the microzones with similar grain sizes. These diverse microzones undergo a special heat treatment during the welding process, resulting in structural transformations that yield distinct microstructural characteristics and associated mechanical properties. Notably, unlike in traditional fusion welding, the subsequent passes in multi-layer and multi-pass welding reheat the previous pass and its heat-affected zone. The weld joint analyzed in this study also demonstrates this phenomenon. The red dot in

Figure 2 indicates the center of the FZ, which will be subject to a detailed microstructure analysis in the following sections.

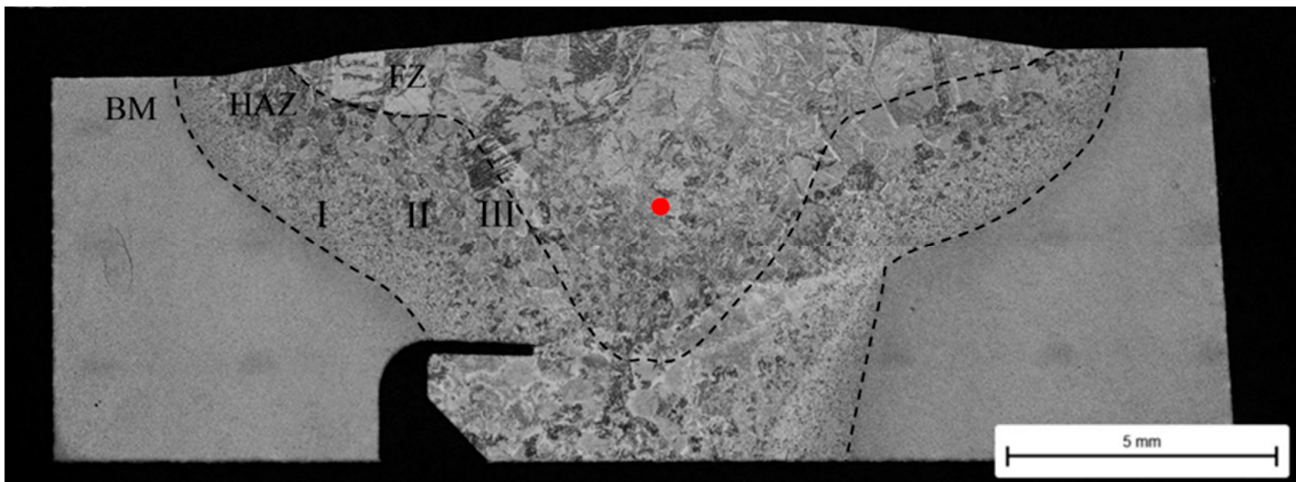


Figure 2. Macrograph of Ti-4Al-2V titanium alloy TIG welding joint. I: the centers of the incomplete recrystallization zone; II: the centers of the recrystallization zone; III: the centers of the superheated zone; and red dot: the centers of the FZ.

3.1. Microstructure of Welded Joint

The microstructures of the various microzones within the BM, HAZ, and FZ are shown in Figure 3, corresponding precisely to the marked positions in Figure 2. As shown in Figure 3a, the Ti-4Al-2V titanium alloy base metal is composed of equiaxed grains at the α phase. In Figure 3b, the microstructure adjacent to the BM, namely, the incomplete recrystallization zone of the HAZ, exhibits notable growth and deformation of the equiaxed α grains, attributable to the influence of the welding heat. This region is less affected by the welding heat and the temperature is below the phase transition temperature, thus causing the grain to increase without a transition of phases. Figure 3c shows that the recrystallization zone of the HAZ is a basket-weave microstructure. Here, the original β grains exhibit irregular shapes, with lamellar α phases and serrated α structures crisscrossing within the grains [26]. In Figure 3d, the microstructure of the superheated zone of the HAZ, characterized by a Widmanstätten structure, is displayed. This zone experiences the highest temperatures within the entire HAZ, exceeding the β transition temperature and approaching the melting point [27]. Specifically, the microstructure reveals distinct features: the grain boundaries of the coarse primary β grains are clear and complete, and there is a grain boundary α phase around the primary β grains. Within these β grains, a larger and parallel flake α phase is observable.

Figure 3e presents the microstructure of the FZ, precisely corresponding to the marked position (the red dot) in Figure 2. During the welding process, the temperature within the FZ exceeds the melting point of the Ti-4Al-2V titanium alloy. As the temperature subsequently decreases, the weld pool commences solidification, leading to the development of coarse β grains. The phase transition of the β phase occurs with a further decrease in temperature, and the secondary α is formed. As evident from the figure, the FZ is primarily constituted of a coarse, irregular, and blocky secondary α phase, accompanied by a minor presence of an acicular martensite α' phase. In the FZ of the Ti-6Al-4V titanium alloy TIG welded joint, a higher concentration of the acicular martensitic α' phase is observed [17,18], whereas in the FZ of the Ti-4Al-2V titanium alloy studied here, there is a lesser amount of the acicular martensitic α' phase. This disparity can be attributed to the adoption of a multi-layer and multi-channel TIG welding process in this research, which results in a slower cooling rate in the fusion zone. Due to this slower cooling, a greater proportion of the β phase transforms into the secondary α phase, with only a minor fraction transforming into the acicular martensite α' phase.

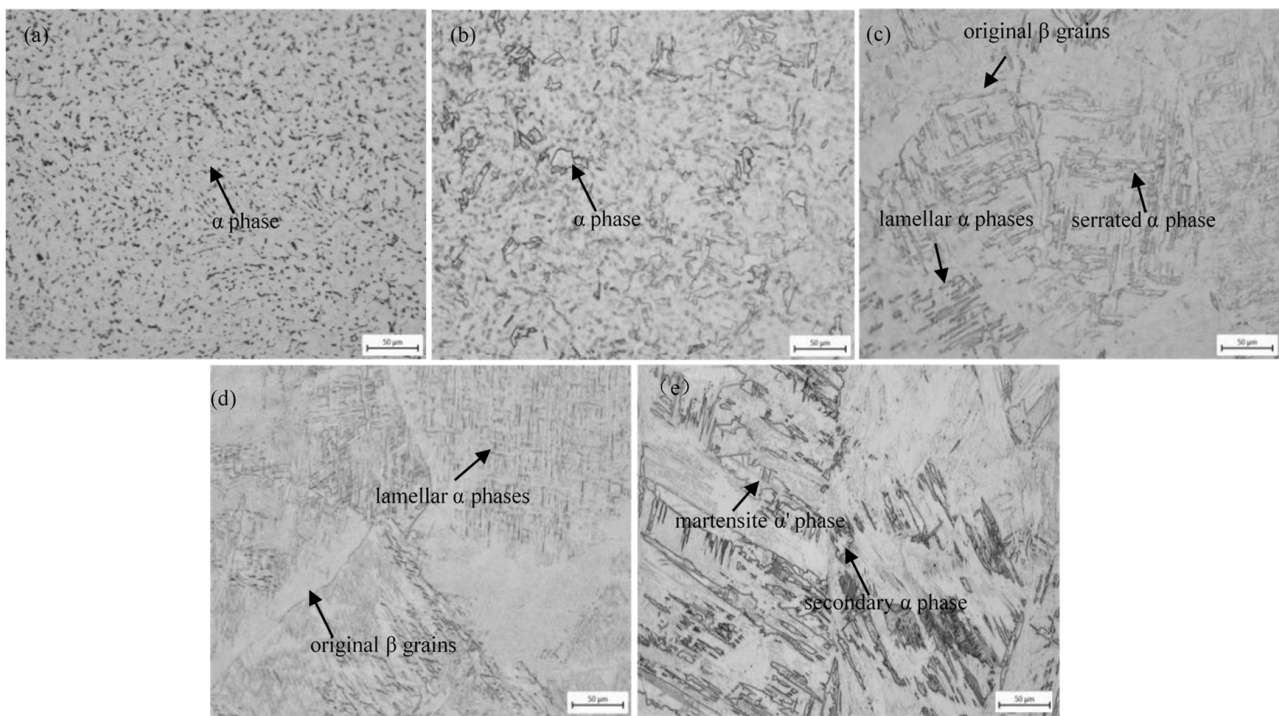


Figure 3. Microstructure of different microzones in the HAZ and FZ: (a) BM, (b) HAZ–incomplete recrystallization zone, (c) HAZ–recrystallization zone, (d) HAZ–superheated zone, and (e) FZ.

Figure 4 shows the inverse pole figure (IPF) of various microzones within the welded joint, while Figure 5 presents the corresponding grain size distributions. As shown in Figure 4, the equiaxed grains of the Ti-4Al-2V titanium alloy base alloy undergo gradual growth and recrystallization due to the influence of the welding thermal cycles. Figure 5a indicates that the grain size of the base alloy spans a range from 5 μm to 10 μm . A comparative analysis of Figure 4b–d reveals that the grains in the recrystallization zone and the superheated zone exhibit a distinct preferred orientation, whereas the grains in the incomplete recrystallization zone lack a preferred orientation. As depicted in Figure 5b–d, the grain sizes in these three microregions primarily vary from 5 μm to 15 μm . Notably, the proportion of grain sizes smaller than 10 μm is 72.32% in the incomplete recrystallization zone, 65.91% in the recrystallization zone, and 55.14% in the superheated zone. The grain size within the FZ is primarily distributed between 10 μm and 20 μm (Figure 5e), with a 26.09% proportion of grains exhibiting sizes smaller than 10 μm .

3.2. Nanoindentation Test of Welded Joint

The load–depth curves obtained from the nanoindentation test conducted on the Ti-4Al-2V titanium alloy welded joint are depicted in Figure 6. By employing the load–displacement (p - h) curve fitting approach methodology by Oliver and Pharr, some important empirical equations were obtained to further understand the principle of this technique [19,20,28]. From the p - h curve, three vital quantities can be extracted: the maximum load (P_{max}), the maximum displacement (h_{max}), and the elastic unloading stiffness ($S = dp/dh$), which is determined from the upper portion of the unloading curve. The hardness (H) and Young’s modulus (E) can be calculated using the following equations [22]:

$$H = \frac{P_{max}}{A} \quad (1)$$

$$S = \frac{2}{\sqrt{\pi}} E_{eff} \sqrt{A} \quad (2)$$

$$\frac{1}{E_{\text{eff}}} = \frac{1 - \nu^2}{E} + \frac{1 - \nu_i^2}{E_i} \tag{3}$$

where A is the contact area; E_{eff} is the effective elastic modulus; and E , ν , E_i , and ν_i are the elastic modulus and Poisson’s ratios of the sample and the indenter, respectively. In this test, $E_i = 1141$ GPa and $\nu_i = 0.07$.

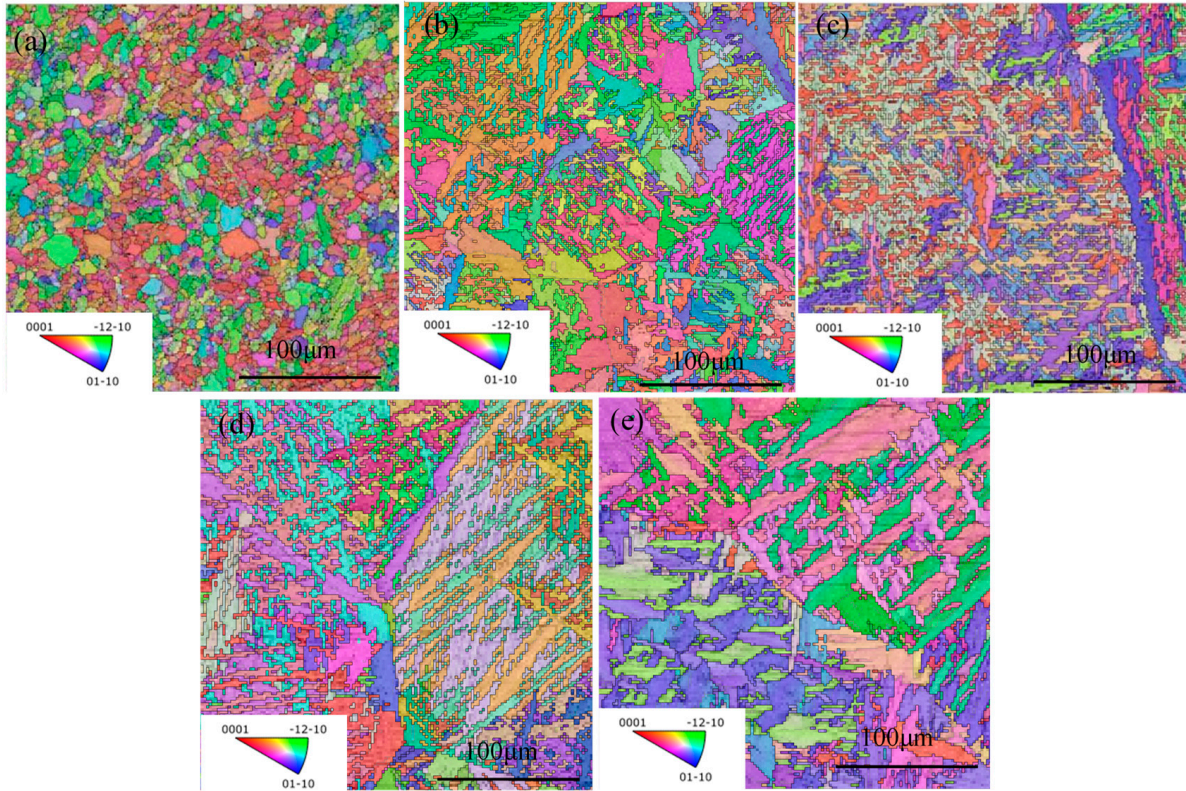


Figure 4. IPF of welded joint: (a) BM, (b) HAZ–incomplete recrystallization zone, (c) HAZ–recrystallization zone, (d) HAZ–superheated zone, and (e) FZ.

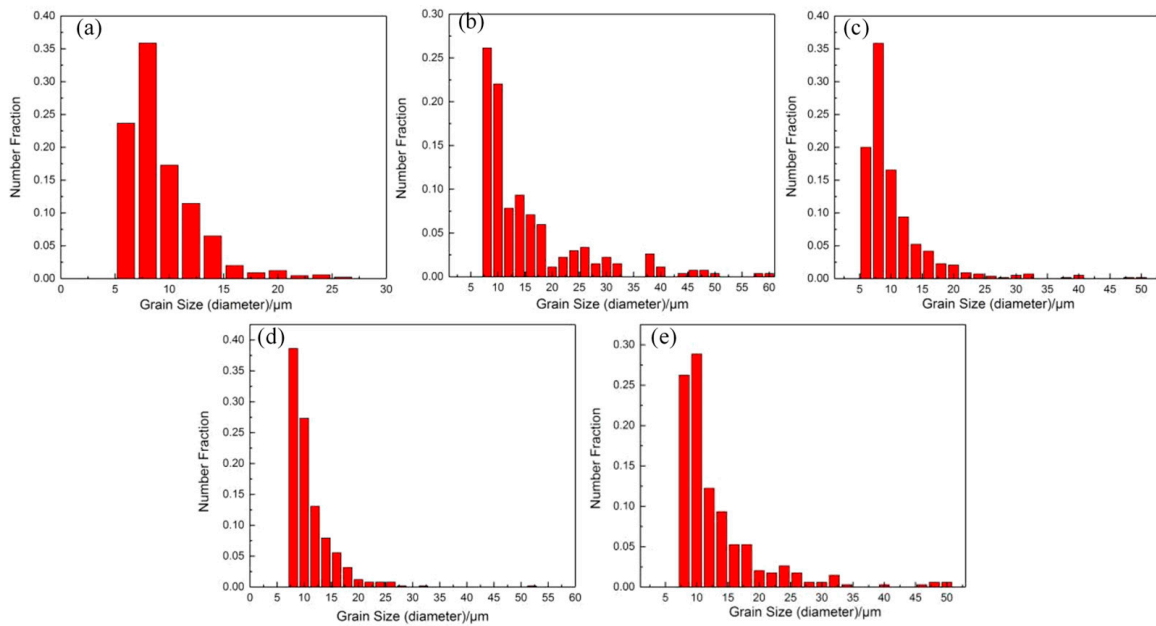


Figure 5. Grain size of welded joint: (a) BM, (b) HAZ–incomplete recrystallization zone, (c) HAZ–recrystallization zone, (d) HAZ–superheated zone, and (e) FZ.

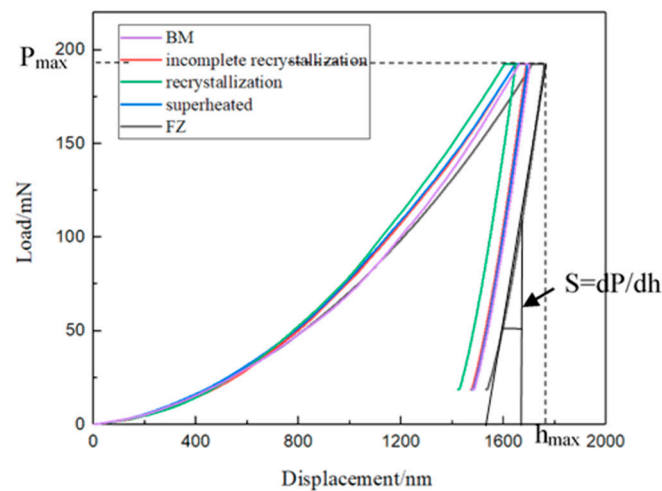


Figure 6. The load–displacement curves of different regions in the welded joint.

As illustrated in Figure 6, the nanoindentation test comprises three distinct stages: loading, holding, and unloading. Notably, for the same applied load, the maximum indentation depth varies significantly across the different microzones of the welded joint. The test results presented in Figure 6 are succinctly summarized in Table 3. In Table 3, when loaded to the maximum load of 200 mN, the instantaneous indentation depth of the FZ is the largest, measuring 1789.771 nm, while the instantaneous indentation depth of the HAZ in the recrystallized region is the smallest, at 1644.969 nm. This variation in indentation depths indicates variations in the resistance to indentation, i.e., the hardness, among the different microzones within the welded joint. It is noteworthy that the nanohardness of the Ti-4Al-2V titanium alloy welded joint exhibits a decreasing trend with an increasing indentation depth, which accords with the positive indentation size effect. This phenomenon, also observed in a nanoindentation study of selective laser-melted Ti-6Al-4V titanium alloys, is attributed primarily to the disappearance of continuous grain boundaries [29].

Table 3. The average nanoindentation test results for the different regions of the welded joint.

	BM	HAZ Incomplete Recrystallization Zone	HAZ Recrystallization Zone	HAZ Superheated Zone	FZ
Hardness H/Gpa	3.226	3.563	3.753	3.48	3.058
Maximum pressure depth h_{max} /nm	1754.01	1691.302	1644.969	1694.23	1789.771
Elastic modulus/Gpa	116.019	120.332	120.315	120.798	116.399

Figure 7 presents a nanohardness cloud image of the welded joint of the Ti-4Al-2V titanium alloy. The results of the Vickers hardness measurement of the welded joint of the Ti-4Al-2V titanium alloy are listed in Table 4. Combined with the test results in Table 3, it can be seen that, compared to the BM, which has a nanohardness of 3.226 GPa, the nanohardness within the HAZ of each microzone exhibits a noticeable increase, whereas a decrease in nanohardness is observed in the FZ. Notably, the nanohardness of the recrystallized zone within the HAZ is the largest, reaching 3.753 GPa. The Vickers hardness measurement results are consistent with the change in nanohardness. Within the HAZ, the hardness of each microzone exceeds that of the BM and the FZ. Notably, the recrystallization zone exhibits the highest hardness value, reaching 298.396 HV. According to Liu et al. [30], the inhomogeneity of the α phase and α' phase in the HAZ of the TA15 titanium alloy electron beam welding joint has an impact on its nanohardness. Furthermore, Babu et al. [17] demonstrated that the morphology and size of the α phase in the welded joint plays a crucial role in determining the mechanical properties. As shown in Figure 7, the highest nanohardness value is concentrated in the central region of the HAZ, specifically in the

recrystallization zone. Referring to Figure 3b, it can be seen that this recrystallization zone primarily consists of a basket-weave microstructure, where the α -phase is uniformly and finely distributed. This fine and uniform α -phase structure is more effective at hindering dislocation movements, thereby enhancing hardening behavior. In contrast, the lowest nanohardness values are observed in the center of the FZ. By analyzing its microstructure in Figure 4e, it becomes clear that the FZ exhibits a coarser grain structure compared to other microregions, which accounts for its lower nanohardness.

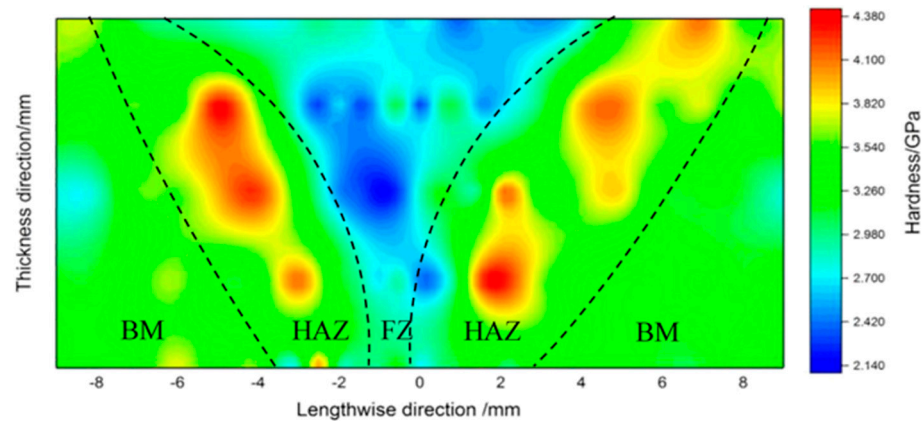


Figure 7. Nanohardness cloud image of the Ti-4Al-2V titanium alloy welded joint.

Table 4. The average Vickers hardness test results for the different regions of the welded joint.

Vickers Hardness	BM	HAZ Incomplete Recrystallization Zone	HAZ Recrystallization Zone	HAZ Superheated Zone	FZ
H/HV	270.754	295.456	298.396	290.042	256.63

As shown in Table 3, the E of every microzone within the HAZ exceeds that of the BM and the FZ. On the other hand, the elastic modulus values of the BM and the FZ closely align with the experimentally determined elastic modulus of the Ti-4Al-2V titanium alloy [31]. The elastic modulus of a material is inherently determined by its crystal properties, specifically reflecting the strength of the interatomic binding forces. Varying values of elastic modulus result in distinct mechanical behaviors at various microscopic scales across different regions. Consequently, the overall performance of the HAZ is superior to that of the other regions.

3.3. Nanoindentation Testing of Typical Microstructures in the HAZ

Figure 8 illustrates the nanoindentation load–depth curves that are representative of the microstructures present in the HAZ. Notably, the basket-weave microstructure depicted in Figure 8b exhibits the highest average nanohardness, achieving a value of 3.93 GPa. Additionally, its elastic modulus is also the highest, attaining 125.191 GPa. The nanohardness trend within the HAZ reveals a distinct hierarchy: basket-weave microstructure > fine-grain microstructure > Widmanstätten microstructure. In a previous study on nanohardness across welded structures of high-strength steel, it was observed that the nanohardness of a fine-grain structure exceeded that of a coarse grain structure [23]. Similarly, this finding aligns with the typical nanohardness variation observed in the microstructure of the Ti-6Al-4V titanium alloy welded joint. A basket-weave microstructure is mainly composed of a fine layer structure; its grain size is small and it has high strength and toughness. The basket-weave microstructure, which primarily comprises fine lamellar structures, exhibit high strength and toughness. The nanoindentation studies conducted on the Ti-6Al-4V titanium alloy reveal that the basket-weave microstructure significantly enhances creep resistance and tensile strength [24,32]. Based on these findings, acquiring a basket-weave microstructure during the welding process is expected to result in a titanium alloy welded

joint with improved mechanical properties. Therefore, achieving a higher proportion of basket-weave microstructures in the Ti-4Al-2V titanium alloy welded joint is desirable.

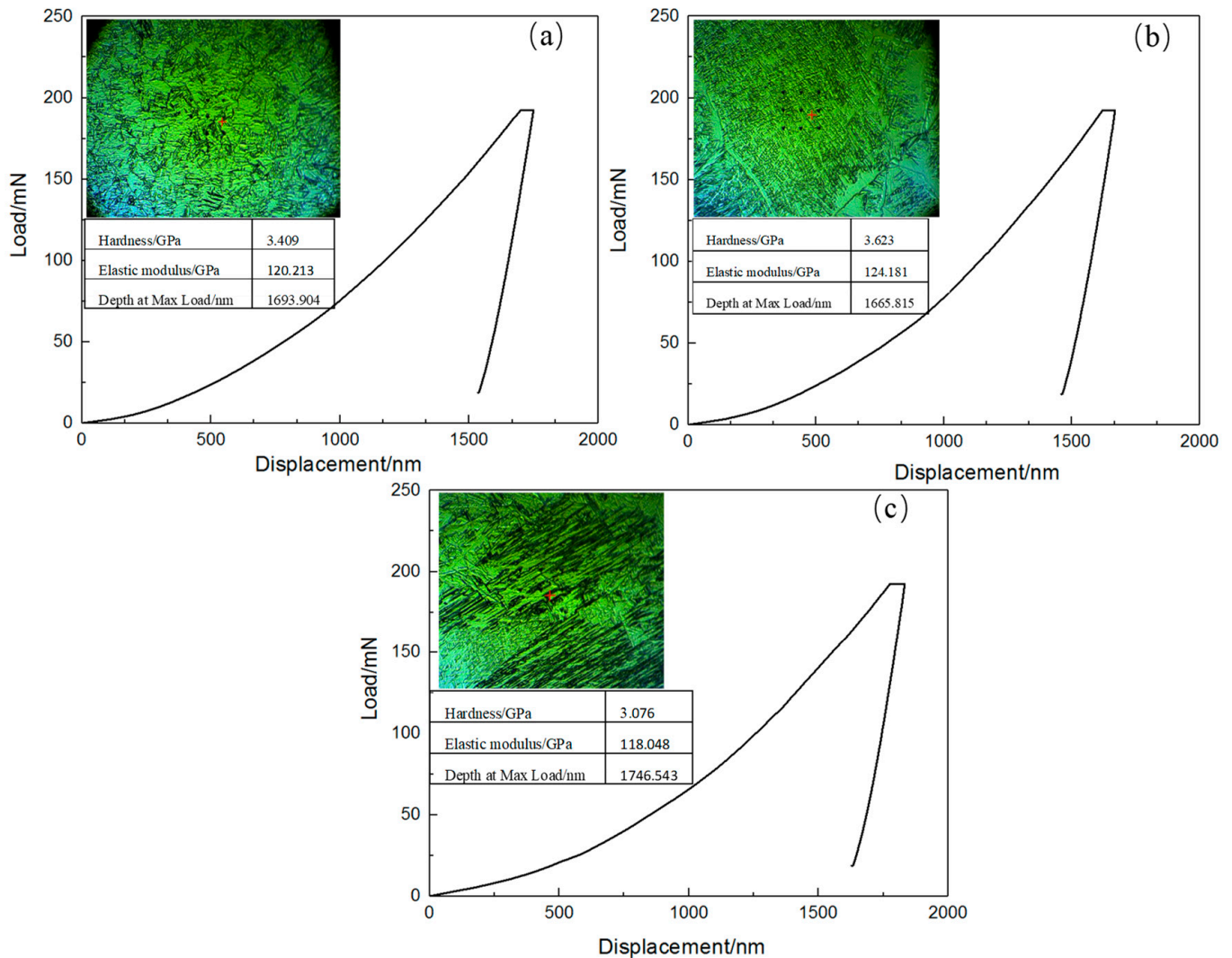


Figure 8. The load–displacement curves of typical microstructures in the HAZ: (a) fine-grain microstructure; (b) basket-weave microstructure; and (c) Widmanstätten microstructure.

4. Conclusions and Future Perspective

Based on the experimental results concerning the microstructural characterizations and mechanical properties of the Ti-4Al-2V titanium alloy TIG weld joint, the following conclusions can be presented:

(1) According to different grain sizes, the HAZ of the Ti-4Al-2V titanium alloy TIG weld joint is categorized into three distinct zones: the incomplete recrystallization zone, the recrystallization zone, and the superheated zone. These zones primarily comprise a grown initial α phase and a secondary lamellar α phase. The FZ is mainly composed of a coarse secondary α phase and an acicular martensite α' phase.

(2) In the recrystallization zone and the superheated zone, the grains exhibit a distinct preferred orientation. Specifically, the proportion of grains with a size less than $10\ \mu\text{m}$ accounts for 65.9% and 55.1%, respectively. Conversely, in the incomplete recrystallization zone, the grains lack a preferred orientation, and the percentage of grains smaller than $10\ \mu\text{m}$ comprises 72.3% of the total grains in that zone.

(3) The average nanohardness values in the various zones of the HAZ are as follows: 3.563 GPa for the incomplete recrystallization zone, 3.753 GPa for the recrystallization zone, and 3.48 GPa for the superheated zone. In contrast, the nanohardness of the FZ is

3.058 GPa. The E of the HAZ is observed to be higher, indicating a superior performance trend compared to the other microzones.

(4) The basket-weave microstructure exhibits the highest average nanohardness, with a value of 3.93 GPa. It is more desirable to obtain a basket-weave structure in the welding process.

In this study, we have conducted an initial examination of the microstructure and properties of the HAZ in the welded joint of a Ti-4Al-2V titanium alloy. This examination has established a relationship between the typical microstructures of the HAZ and their mechanical properties. To further investigate the properties of the different microzones within the next phase of our work will involve utilizing thermal simulation welding technology. This will enable us to obtain independent, large-sized specimens that possess the same microstructure as each microzone of the HAZ. These samples will then be applied to mechanical and corrosion tests to further investigate the mechanical and corrosion properties of each microzone in the HAZ. However, two major challenges remain. Firstly, accurately determining the thermal cycling temperature of each microzone within the HAZ is crucial. Secondly, ensuring the consistency of the microstructure between the thermally simulated samples and the actual welded components is essential to the validity of our findings. Overcoming these challenges will be the focus of our ongoing research.

Author Contributions: Conceptualization, Y.C., S.Z., B.Q., J.W. and L.W.; methodology, Y.C., X.L. and Z.Z.; validation, X.L. and K.W.; investigation, Y.C., Z.Z. and K.W.; writing—original draft, Y.C.; writing—review and editing, S.Z., B.Q. and J.W.; and supervision, B.Q., J.W. and L.W. All authors have read and agreed to the published version of the manuscript.

Funding: This work was supported by the Original Foundation of the Nuclear Power Institute of China (YF9722002), the National Natural Science Foundation of China (52205173), the Natural Science Foundation of Sichuan Province of China (2023NSFSC0912), the Guangdong Basic and Applied Basic Research Foundation (2023A1515110746), and the Shenzhen Science and Technology Program (JCYJ20230807093410021).

Data Availability Statement: The raw data supporting the conclusions of this article will be made available by the authors on request.

Conflicts of Interest: The authors declare no conflicts of interest.

References

1. Donachie, M.J. *Titanium: A Technical Guide*; ASM International: Materials Park, OH, USA, 2000.
2. Oryshchenko, A.S.; Gorynin, I.V.; Leonov, V.P.; Kudryavtsev, A.S.; Mikhailov, V.I.; Chudakov, E.V. Marine Titanium Alloys: Present and Future. *Vopr. Materialoved.* **2015**, *6*, 571–579. [[CrossRef](#)]
3. Rodchenkov, B.S.; Kozlov, A.V.; Kuznetsov, Y.G.; Kalinin, G.M.; Strebkov, Y.S. Irradiation behavior of Ti-4Al-2V (PT-3B) alloy for ITER blanket modules flexible attachment. *J. Nucl. Mater.* **2007**, *367*, 1312–1315. [[CrossRef](#)]
4. Omoniyi, P.; Mahamood, M.; Jen, T.C.; Akinlabi, E. TIG welding of Ti6Al4V alloy: Microstructure, fractography, tensile and microhardness data. *Data Brief* **2021**, *38*, 107274. [[CrossRef](#)] [[PubMed](#)]
5. Yi, H.J.; Lee, Y.J.; Lee, K.O. TIG Dressing Effects on Weld Pores and Pore Cracking of Titanium Weldments. *Materials* **2016**, *6*, 243. [[CrossRef](#)]
6. Ou, P.; Cao, Z.; Rong, J.; Yu, X. Molecular Dynamics Study on the Welding Behavior in Dissimilar TC4-TA17 Titanium Alloys. *Materials* **2022**, *15*, 5606. [[CrossRef](#)]
7. Wei, X. TIG Welding of Titanium Alloys. *Titan. Ind. Prog.* **2008**, *25*, 38–41.
8. Górka, J.; Przybyła, M.; Szmul, M.; Chudzio, A.; Ładak, D. Orbital TIG Welding of Titanium Tubes with Perforated Bottom Made of Titanium-Clad Steel. *Adv. Mater. Sci.* **2019**, *19*, 55–56. [[CrossRef](#)]
9. Chen, H.; Guo, L.; Cao, C. Hot deformation behavior and microstructure evolution of TC11 alloy with lamellar structure. *J. Aeronaut. Mater.* **2008**, *28*, 18–22.
10. Zhou, Y.; Zeng, W.; Li, X.; Yu, H.; Cao, C. An investigation of high-temperature deformation strengthening and toughening mechanism of titanium alloy. *Acta Metall. Sin.* **1999**, *35*, 45–48.
11. Zhang, W.F.; Wang, Y.H.; Li, Y.; Ma, J.M. Phase transformation, microstructures and tensile properties of TA15 titanium alloy. *Chin. J. Nonferrous Met.* **2010**, *20*, s523–s528.
12. Kumar, K.; Masanta, M.; Sahoo, S.K. Microstructure evolution and metallurgical characteristic of bead-on-plate TIG welding of Ti-6Al-4V alloy. *J. Mater. Process. Technol.* **2019**, *265*, 34–43. [[CrossRef](#)]

13. Fu, C.; Wang, Y.; He, S.; Zhang, C.; Jing, X. Microstructural characterization and mechanical properties of TIG weld joint made by forged Ti-4Al-2V alloy. *Mater. Sci. Eng. A* **2021**, *821*, 141604. [[CrossRef](#)]
14. Sundaresan, S.; Ram, G.J.; Reddy, G.M. Microstructural refinement of weld fusion zones in alpha-beta titanium alloy using pulsed current welding. *Mater. Sci. Eng. A* **1999**, *262*, 88–100. [[CrossRef](#)]
15. Akhonin, S.V.; Belous, V.Y.; Berezos, V.A.; Selin, R.V. Effect of TIG-Welding on the Structure and Mechanical Properties of the Pseudo- β Titanium Alloy VT19 Welded Joints. *Mater. Sci. Forum* **2018**, *927*, 112–118. [[CrossRef](#)]
16. Hu, J.; Hu, Y.; Zeng, C.; Zhang, Y.; Dong, C. Microstructure and Mechanical Properties of Welded Joints of TA17 Ti Alloy by Magnetically Controlled Narrow-Gap TIG Welding. *Hot Work. Technol.* **2023**, *52*, 42–50.
17. Babu, N.K.; Raman SG, S.; Mythili, R.; Saroja, S. Correlation of microstructure with mechanical properties of TIG weldments of Ti-6Al-4V made with and without current pulsing. *Mater. Charact.* **2007**, *58*, 581–587. [[CrossRef](#)]
18. Mehdi, B.; Badji, R.; Ji, V.; Allili, B.; Bradai, D.; Deschaux-Beaume, F.; Soulié, F. Microstructure and residual stresses in Ti-6Al-4V alloy pulsed and unpulsed TIG welds. *J. Mater. Process. Technol.* **2016**, *231*, 441–448. [[CrossRef](#)]
19. Gao, D.; Yao, Y.; Yuan, Z. Study on micro-hardness testing of materials. *Aviat. Precis. Manuf. Technol.* **2001**, *37*, 7–10.
20. Vannod, J.; Bornert, M.; Bidaux, J.E.; Bataillard, L.; Karimi, A.; Drezet, J.M.; Rappaz, M.; Hessler-Wyser, A. Mechanical and microstructural integrity of nickel-titanium and stainless steel laser joined wires. *Acta Mater.* **2011**, *59*, 6538–6546. [[CrossRef](#)]
21. Chu, Q.; Zhang, M.; Li, J.; He, X. Microstructure and nanoindentation investigation of Q345-Zr-Q345 welded joint. *Welded Pipe Tube* **2018**, *41*, 9–14.
22. Deng, C.Y.; Ce, L.I.U.; Gong, B.M.; Zhang, C.Z.; Chang, L.I.U.; Yong, L.I.U. Effect of microstructure inhomogeneity on mechanical properties of different zones in TA15 electron beam welded joints. *Trans. Nonferrous Met. Soc. China* **2020**, *30*, 678–687. [[CrossRef](#)]
23. Lan, L.Y.; Qiu, C.L.; Zhao, D.W. Analysis of the hardness and elastic modulus distribution in a high strength steel welded joint by nanoindentation. *Adv. Mater. Res.* **2011**, *189*, 3270–3273. [[CrossRef](#)]
24. Chen, Z.; Wang, B.; Duan, B. Mechanical properties and microstructure of a high-power laser-welded Ti-6Al-4V titanium alloy. *J. Mater. Eng. Perform.* **2020**, *29*, 2296–2304. [[CrossRef](#)]
25. Hassaan, M.; Junaid, M.; Shahbaz, T.; Ilyas, M.; Khan, F.N.; Haider, J. Nanomechanical response of pulsed tungsten inert gas welded titanium alloy by nanoindentation and atomic force microscopy. *J. Mater. Eng. Perform.* **2021**, *30*, 1490–1503. [[CrossRef](#)]
26. Zhao, Y.Q.; Chen, Y.N.; Zhang, X.M.; Zeng, W.D.; Wang, L. *Phase Transformation and Heat Treatment of Titanium Alloy*; Central South University Press: Changsha, China, 2012.
27. Wu, H.; Feng, J.; He, J. Microstructure evolution and fracture behavior for electron beam welding of Ti-6Al-4V. *Bull. Mater. Sci.* **2004**, *27*, 387–392.
28. Oliver, W.C.; Pharr, G.M. An improved technique for determining hardness and elastic modulus using load and displacement sensing indentation experiment. *J. Mater. Res.* **1992**, *7*, 1564–1583. [[CrossRef](#)]
29. Tian, X.; Yang, S.; Dong, G.; Jang, A.; Lang, F.; Li, J. Size effect analysis in nanoindentation of Ti-6Al-4V alloy prepared by selective laser melting. *Nonferrous Met. Eng.* **2021**, *11*, 19–25.
30. Liu, C.; Deng, C.; Gong, B.; Zhang, C. Effects of microstructure inhomogeneity on strain concentration of heat affected zone of TA15 titanium alloy electron beam weld joint. *Trans. China Weld. Inst.* **2019**, *40*, 49–52.
31. Wang, X. *Progress in Nuclear Fuel and Materials Research 1992–2012*; Sichuan University Press: Chengdu, China, 2012.
32. Dong, G.; Yang, S.; Jang, A.; Lang, F.; Tian, X.; Li, J. Nanoindentation creep of Ti-6Al-4V alloy prepared by selective laser melting. *Surf. Technol.* **2020**, *49*, 252–259.

Disclaimer/Publisher's Note: The statements, opinions and data contained in all publications are solely those of the individual author(s) and contributor(s) and not of MDPI and/or the editor(s). MDPI and/or the editor(s) disclaim responsibility for any injury to people or property resulting from any ideas, methods, instructions or products referred to in the content.